3D printed multi-functional scaffolds based on poly(ε-caprolactone) and hydroxyapatite composite

Fan Liu
Wuhan Institute of Technology https://orcid.org/0000-0002-2865-2372
Honglei Kang
Huazhong University of Science and Technology
Zhiwei Liu
Wuhan Institute of Technology
Siyang Jin
Wuhan University of Technology
Guoping Yan (guopyan2006@163.com)
Wuhan Institute of Technology https://orcid.org/0000-0002-2649-9108
Yunlong Sun
Huazhong University of Science and Technology
Feng Li (lifengmd@hust.edu.cn)
Huazhong University of Science and Technology
Haifei Zhan
Queensland University of Technology
Yuantong Gu
Queensland University of Technology

Research

Keywords: poly(ε-caprolactone), hydroxyapatite, biodegradability, 3D printed scaffolds, bone tissue regeneration

Posted Date: May 13th, 2021

DOI: https://doi.org/10.21203/rs.3.rs-486510/v1

Abstract

Background: Biodegradable polymeric scaffolds are critical to repair a large bone defect, which can provide a porous and network microenvironment for cell attachment and bone tissue regeneration. A multifunctional biodegradable PCL/HA composite was prepared with the blending of poly(ε-caprolactone) (PCL) and hydroxyapatite nanoparticles (HA). Subsequently, the PCL/HA scaffolds implants were produced by the screw extrusion/melting deposition forming method using PCL/HA composite as a raw material in this work.

Results: Through a serial of *in vitro* assessments, it is found that the PCL/HA composite possesses good biodegradability, good biocompatibility, and steady drug release performance, which can improve the cell proliferation of osteoblast cells MC3T3-E1. Meanwhile, *in vivo* experiments were carried out for the rats with skull defect and rabbits with bone defects. It is observed that the PCL/HA scaffolds implants allow the adhesion and penetration of bone cells, which enables the growth of bone cells and bone tissue regeneration. With a composite design to load an anticancer drug and achieve sustained drug release, the scaffolds could enhance bone repair and be expected to inhibit the tumor cells and improve patient outcomes.

Conclusions: This work signifies that PCL/HA composite can be used as the potential biodegradable scaffolds for bone repairing after bone malignant tumor resection.

1. Introduction

Due to the losing of osteogenic microenvironment, it is a great clinical challenge to repair a large bone defect [1–3]. Biodegradable polymeric scaffolds possess porous and network structures, which provide the matrix and microenvironment for cell attachment and bone tissue regeneration. In particular these polymeric scaffolds do not need to be removed by second operation since polymers can be completely degraded *in vivo* [4–6]. Biodegradable aliphatic polyesters, such as poly(lactic acid) (PLA), poly(ε-caprolactone) (PCL), and poly(trimethyl carbonate) are the attractive polymers that have been widely used as the tissue engineering matrix and drug controlled release system [7–9]. Specifically, PCL is a preferred synthetic aliphatic polyester biomaterial due to their good biodegradability and biocompatibility, low toxicity, and weak inflammatory effect of the degraded products. It has been shown to be suitable for the fabrication of biodegradable scaffolds for tissue regeneration and tissue engineering [10–12].

The polymer composites containing nanoceramics were reported to possess better mechanical properties than that of the pure polymers due to additional strength and stiffness provided by the embedded ceramic nanoparticles. As such, the polymer composite-based scaffolds can withstand a certain level of physiological loading and function before the new tissue replaces the scaffold matrix (during its gradual degrading process) [13, 14]. Hydroxyapatite (HA) is a naturally occurring mineral form of calcium apatite and an important component of human skeleton and teeth. It has been widely applied as the good bone grafting material, replacement and supplement material because of its convenient production, low

toxicity, good biocompatibility and high bioactivity [15, 16]. Thus it is of great interest to explore whether HA can be applied as reinforcements for PCL in biomedical applications.

In the prosthodontic treatment of bone defects, the ideally implanted scaffolds should be biodegradable while new bone tissue is growing. They should have good bioactivity to promote the bone-binding ability, and possess other biological actions such as antitumor, antiangiogenic, anti-collagenolytic and anti-inflammatory properties for bone regeneration. Recently, some physical and chemical methods (such as surface functionalization and blending) were used to fabricate functional scaffold materials for tissue engineering applications. For instance, Sarkar et al. [17] fabricated calcium phosphate (CaP) scaffolds with the encapsulation of hydrophobic biomolecule curcumin (within a liposome), which eradicate the osteosarcoma cells and also promote osteoblast proliferation, offering new opportunities to treat bone defects after tumor resection.

This work prepared a polymer composite based on poly(ε-caprolactone) and hydroxyapatite with the addition of doxorubicin (DOX) as an anticancer drug. DOX was chosen as a model drug due to its widespread use in bone cancer. Biodegradable scaffolds were further fabricated based on this polymer composite using screw extrusion/melting deposition forming approach. The polymer composite was also evaluated to be used as the potential biodegradable scaffolds for bone repairing.

2. Materials And Methods

2.1. Materials

All chemicals and solvents were of analytical grade. Toluene and tetrahydrofuran (THF) were purified by redistillation over sodium. Triethylamine was refluxed under phthalic anhydride and dried over calcium hydride (CaH_2) before use. Tin (II) 2-ethylhexanoate ($Sn(Oct)_2$) was purchased from Sigma-Aldrich (Louis, MO, United States of America) and purified by redistillation in vacuo before use. PCL was synthesized by ring-opening bulk polymerization of ε-caprolactone using $Sn(Oct)_2$ as a catalyst [18–20]. PCL was characterized by the gel permeation chromatography, ^1H NMR, Fourier transform infrared spectroscopy, UV, differential scanning calorimetry, and automatic contact-angle measurements. PCL: ^1H NMR (300MHz, $CDCl_3$, δ, ppm): 4.25 (m, 4H, C-C**H**$_2$), 2.06 (m, 2H, C-C**H**$_2$-C). FT-IR (KBr,cm^{-1}): 3450 (OH), 2963, 2922 (C-C), 1740 (C = O), 1461 (C-C), 1172, 1034 (C-O). The molecular weight (M_n) was 1.94×10^5 and polydispersity was 1.47 as determined by Gel Permeation Chromatography (GPC, Waters Corporation Milford, MA, United States of America). Hydroxyapatite (HA) nanoparticles with average diameter of particle sizes of 20 nm were purchased from the Beijing Deke Daojin Science and Technology Co., Ltd. (Beijing, China).

2.2.1 Instrumentation

The compounds were characterized using a UV-Vis spectrophotometer (UV-2800 series, Unico, Shanghai, China), a Nicolet is10 Fourier Transform-Infrared (FT-IR) spectrophotometer (Thermo Fisher Scientific Inc.,

Madison, WI, United States of America), a Varian Mercury-VX300 NMR spectrometer (Varian, Inc. Corporate, Palo Alto, CA, United States of American) and an automatic contact angle meter (SL200A/B/D Series, Solon Tech. Inc. Ltd., Shanghai, China). The molecular weight was measured by a gel permeation chromatography (GPC, Waters Corporation Milford, MA, United States of American) (Waters 2965D separations module, Waters 2414 Refractive Index Detector, Shodex K802.5 & K805 with Shodex K-G Guard Column, Polystyrene Standard, DMF solvent, 1.0 mL.min^{-1} flow rate, 323K Column temperature and 323K Detector temperature). The glass transition temperature (Tg) was measured by a differential scanning calorimeter (DSC) (NETZSCH DSC 200 F3, Erich NETZSCH GmbH & Co. Holding KG, Gebrüder-Netzsch-Strasse, Selb, Germany). The morphologies were characterized using a SEM (JEOL JSM-7001F, Japan) at 5–10 kV. Before SEM observation, the specimens were gold-sputter coated using an auto fine coater (JEOL, Ltd., Japan) under argon atmosphere for 60 s. The elemental distribution of calcium (Ca), phosphorus (P), oxygen (O), and carbon (C) in the scaffolds was investigated using an EDS (Phenom World BV, Netherlands). The phase composition was investigated using a XRD diffractometer (German Bruker Co., Germany) with Cu Ka radiation (λ = 0.154056 nm, 40 kV, 40 mA). Before analysis, the scaffold specimens were fixed on a specimen holder by double side adhesive tape. The data were recorded in the 2θ range of 10–75° with scanning speed of 8° min^{-1}. The absorbance (optical density: OD_{492}) were measured with a DG-3022A ELISA-Reader (Hercules, CA, United States of American). The osteoblast cells MC3T3-E1 were provided by the China Center for Type Culture Collection of Wuhan University, China. The ethical approval was obtained for the *in vivo* experiments in animals from the Department of Science and Technology of Hubei Province, China and the Animal Center of Tongji Medical College, Huazhong University of Science and Technology, China.

2.3. Preparation of poly(ε-caprolactone) and hydroxyapatite (PCL/HA) scaffolds

Two different types of composite (PCL/HA and PCL/HA/DOX) samples were prepared, with one containing PCL and HA and the other one containing PCL, HA and doxorubicin (DOX). The dichloromethane was used to ensure even mixture between PCL and HA (or DOX). The mixture was slowly evaporated to dry under reduced pressure. The residue was cut into small pieces and dried under vacuum for 48 h to yield PCL/HA composite and PCL/HA/DOX composite.

Thereafter, the 3D printed PCL/HA scaffolds (diameter: 4 mm and height: 6 mm; diameter: 10 mm and height: 2 mm) and multi-functional PCL/HA/DOX scaffolds containing DOX (diameter: 4 mm and height: 6 mm) were prepared by the screw extrusion/melting deposition forming method using a 3D printer of melting deposition forming (Hubei Joye 3D High-tech Co., Ltd., Chibi, Hubei Province, China) with PCL/HA and PCL/HA/DOX composites as raw materials, respectively. The printing conditions were listed as follows: the printing temperature was 130^{o}C and preheating temperature of the operation desk was 50^{o}C, the nozzle aperture was ≥ 0.4 mm, the extrusion speed was 220 mm/min, and the printing rate was 70 mm/s. *In vivo* implanted PCL/HA scaffolds in a thigh-bone defect model of lower limb in rabbits were further loaded of 3D printed PCL/HA scaffolds and multi-functional PCL/HA/DOX scaffolds by collagen I respectively according to the method cited in the literatures. [22–24]

2.4. In vitro degradation test

PCL and PCL/HA scaffolds (0.1g, diameter: 10 mm and height: 2 mm) were prepared as above and then dried *in vacuum* for 24 h. The scaffolds were suspended in 10 mL of PBS in a dialysis bag. The dialysis bag was sealed and then slowly shaken in 90 mL of PBS (pH 7.4) at 37^{o}C in a 250 mL Erlenmeyer flask. At predetermined time intervals, the samples were taken out of the degradation medium, rinsed with distilled water and then dried *in vacuo* for 48 h. The molecular weight, water absorption and weight loss were calculated, respectively.

The PCL/HA samples for mechanics testing were further prepared by the thermoforming of PCL/HA composite materials in a standard mold on an injection molding machine. *In vitro* degradation test was also measured using PCL/HA samples according to the above same method as PCL/HA scaffolds.

2.5. In vitro drug release study

Doxorubicin (DOX, 10 mg) and PCL or PCL/HA composite materials (100 mg) were dissolved in 20 mL of THF. The solution was homogenized by sonication for 30s and then allowed to evaporate. The resulting film was cut into small pieces and dried under vacuum for 48 h to obtain 5-DOX-incorporated PCL or PCL/HA composite materials. The 5-DOX-incorporated PCL or PCL/HA scaffolds were further prepared by the thermoforming of 5-DOX-incorporated PCL or PCL/HA composite materials in a disc mold (diameter: 10 mm and height: 2 mm) on a thermocompressor with loading pressure of 10 MPa, setting temperature of 110^{o}C and molding time of 10 min.

The 5-DOX-incorporated PCL or PCL/HA scaffolds were suspended in 10 mL of PBS in a dialysis bag. The dialysis bag was sealed and then slowly shaken in 90 mL of PBS at 37^{o}C in a 250-mL Erlenmeyer flask. Aliqouts of the solution outside the dialysis membrane (25 mL) were replaced with 25 mL of PBS at various times intervals and tested at 256 nm by a high-performance liquid chromatography spectrophotometer (HPLC). The changes of the concentrations of DOX were obtained from curves of the absorption *A* versus concentration *C* of DOX in PBS on the basis of Lambert-Beer law.

2.6. Cell viability and proliferation assay

The circular 3D printed PCL and PCL/HA scaffolds (diameter: 10 mm, thickness: 2 mm, the content of HA: 5%, 10%, 15%, 20% and 25%) were placed into the wells of 24 wells plate. The scaffolds were sterilized using Ultraviolet light for 1 hour for each side and secured with a stainless-steel ring. MC3T3-E1 cells were seeded onto the scaffolds at a density of 4×10^4 cells/mL and 100 μL of the RPMI-1640 growth medium was added. Cell counting kit 8 (CCK-8) assay was performed on 1 and 3 days after culture. The cells were incubated for 1 and 3 days in an incubator (37^{o}C, 5% CO_2) and the medium was replaced by the fresh growth medium. And then 10μL of CCK-8 solution was added to each well and continued incubating for 3 hours. The absorbance (optical density: OD_{492}) was measured at 492 nm with a DG-3022A ELISA-Reader and expressed as a percentage relative to control cells (no scaffolds).

2.7. In vivo implanted assay of PCL/HA scaffolds in skull defect and histological analysis

Eighteen 6-week-old SD rats were divided into three groups (control, PCL and PCL/HA, for each group, n = 6) and the circular skull defect model (diameter of about 10 mm) was made in the head of each rat. Subsequently the rat was anesthetized with urethane (10%, 10mL/kg), positioned prone and fixed to a polystyrene cradle with adhesive tape to minimize motion. The scalp along the sagittal suture was shaved and the skin was sterilized with iodine. A 15 mm long incision along the sagittal suture was made, and then, the calvarial bone was exposed by blunt dissection. A 10 mm diameter defect was created using a trephine bur (3i Implant Innovation, Palm Beach Gardens, FL, United States of America) on left parietal bone. The circular scaffolds of 10 mm diameter were was sterilized with UV light for 1 hour for each side and implanted into the bone defects for each group (PCL and PCL/HA scaffolds). For the control group, the rats were treated the same and but without implantation. The periosteum and the overlying skin were then stitched up using the nylon suture. After one month postsurgery, the rats were anesthetized and perfused through heart by using 4% paraformaldehyde. The whole calvaria was harvested and further fixed with 4% paraformaldehyde at room temperature for 2 days for the following evaluations. To assess the new bone formation in the bone defeat area, micro-computed tomography (micro-CT) (micro-CT 50, Scanco Medical AG, Bassersdorf, Switzerland) was applied under the fixed conditions (24 kV, 2 mA, 90 seconds). Area of new bone formation and percentage were measured using the Image Processing and Analysis in Java (ImageJ-1.51r, NIH, United States of America) software.

Nine 6-week-old SD rats were divided into three groups (control, PCL and PCL/HA scaffolds, for each group, n = 3) and anesthetized with urethane (10%, 10mL/kg), positioned prone and fixed to a polystyrene cradle with adhesive tape to minimize motion. The scalp along the sagittal suture was shaved and the skin was sterilized with iodine. A 15 mm long incision along the sagittal suture was made in the muscle on the back. The circular scaffolds of 10 mm diameter were was sterilized with UV light for 1 hour for each side and implanted into the muscle defects for each rat (PCL and PCL/HA scaffolds). For the control group, the rats were treated the same and but without implantation. The periosteum and the overlying skin were then stitched up using the nylon suture. After 3 days postsurgery, the rats were anesthetized and the circular scaffolds were moved. The samples of muscle tissues around scaffolds were taken out and embedded in paraffin and sectioned at a thickness of 5 μm for Hematoxylin-eosin (H&E) staining. The H&E staining slides were observed under an optical microscope, and the images were captured under an IX-70 fluorescence inverted microscope (Olmypus Co., Ltd., Japan). Histological evaluation was performed by two independent examiners.

2.8. In vivo implanted assay of PCL/HA scaffolds in thigh-bone defect

The 3D PCL/HA scaffolds containing collagen I and multi-functional PCL/HA/DOX scaffolds containing collagen I and DOX (diameter: 4 mm and height: 6 mm) were further produced by the loading of 3D printed PCL/HA scaffolds and multi-functional PCL/HA/DOX scaffolds with collagen I accordingly to the

methods in cited literatures respectively. Eighteen 6-week-old New Zealand white rabbits were divided into three groups (control, PCL/HA scaffolds with 25% HA content loading of collagen I and multi-functional PCL/HA scaffolds with 25% HA content loading of collagen I and DOX, for each group, n = 6) and the circular thigh-bone defect model (diameter of about 4 mm) was made in each rat. Subsequently the rabbits was anesthetized with urethane (10%, 10mL/kg), positioned prone and fixed to a polystyrene cradle with adhesive tape to minimize motion. The scalp along the sagittal suture was shaved and the skin was sterilized with iodine. A 15 mm long incision along the sagittal suture was made, and then, the thigh-bone was exposed and a 4 mm diameter defect was created using a trephine bur in the cancellous bone. The scaffolds (diameter: 4 mm and height: 6 mm) were sterilized with UV light for 1 hour for each side and implanted into the bone defects for each group. For the control group, the rats were treated the same and but without implantation. The periosteum and the overlying skin were then stitched up using the nylon suture. After 2 months postsurgery, the rabbits were anesthetized and perfused through heart by using 4% paraformaldehyde. The whole thigh-bone was harvested and further fixed with 4% paraformaldehyde at room temperature for 2 days for the following evaluations.

The new bone formation in the bone defeat area was assessed using micro-computed tomography (micro-CT) (Skyscan1276 X-Ray Microtomograph (Micro CT), Bruker, Belgium) under the fixed conditions (voltage: 93 kv, current: 800 μA, scanning resolution: 6.5 μm). Area of new bone formation and percentage were measured using the Image Processing and Analysis software in the Skyscan1174 Micro CT Scanner with taking the femoral implant as the reference baseline. The cylindrical area with a diameter of 4.1 mm and a thickness of 6 mm was set as the three-dimensional reconstruction area of interest (ROI). The three-dimensional image was reconstructed with N-Recon software and the three-dimensional analysis was performed with CT-AN software. Moreover, the bone mineral density (BMD) of the new bone area was also measured.

2.9. Statistical analysis

All results were expressed as mean differences and were tested for significance by a *t* test, $P < 0.05$ being considered a significant difference.

3. Results And Discussion

3.1. Characterization

The micrographs of PCL/HA scaffolds were examined by scanning electron microscopy (SEM, JEOL JSM-7001F, Japan) at 5–10 kV and the specimens were coated with gold-sputter using an auto fine coater (JEOL, Ltd., Japan) under argon atmosphere for 60 s. As shown in Fig. 1a, HA nanoparticles scatter uniformity in the scaffolds with some aggregated occasions. Uniform pore with different diameters is observed from the 3D printed PCL/HA scaffolds. Figure 1b shows the mapping distribution of C, O, Ca, and P elements in the HA powders, which appears uniformly distribute in the scaffolds. Herein, the elemental distribution in the scaffolds is investigated using an EDS (Phenom World BV, Netherlands).

In this work, PCL/HA scaffolds with 400–800 nm of uniform pore sizes are chosen as the implanted samples as such pore size is expected to be beneficial for cell proliferation/differentiation *in vivo*.

Chemical characterization of pure PCL, HA and PCL/HA scaffolds with different content of HA were conducted by a Nicolet is10 Fourier Transform-Infrared (FT-IR) spectrophotometer (Thermo Fisher Scientific Inc., Madison, WI, United States of America) and their characteristic peaks are shown in Fig. 2a. For the composite samples, many of the absorption bands are overlapped but the properties of the functional groups remain unchanged. Whereas, the shape, location and intensity of the spectral peaks change significantly. The spectra of PCL/HA scaffolds show typical ester peaks (at 1724 cm^{-1}, 1640 cm^{-1}) and CH peaks (2923 cm^{-1}). The increase of HA content in the scaffolds (from 0 to 25%) decreases the peak intensities. Specifically, PCL/HA scaffolds show spectral features in the range of 1150 and 960 cm^{-1}, which are related to the P-O and P = O vibrations of HA. The peak intensities of the spectral range of 3500 – 3200 cm^{-1} that represents the absorption peak of OH groups of HA, decrease evidently.

Typical X-ray diffraction (XRD) spectra obtain for PCL/HA scaffolds are presented in Fig. 2b. The scaffold specimens were fixed on a specimen holder by double side adhesive tape and the XRD diffractometer (German Bruker Co., Germany) with Cu Ka radiation (λ = 0.154056 nm, 40 kV, 40 mA) was utilized. The data were recorded in the 2θ range of 10° – 75° with a scanning speed of 8 min^{-1}. As illustrated in Fig. 3b, the spectra of PCL/HA scaffolds appear similar as that of pure PCL. In addition to the strong peaks associated with the crystalline PCL phase, relatively weak peaks at ∼25.32°, 32.78°, 41.43°, 45.58° and 46.58° are observed, which correlate to the crystalline HA phase. These observations imply the presences of both PCL and HA in the mixture powders. Combined with the above SEM image in Fig. 2a, these observations indicate that the fine HA nanocrystals are well dispersed in the PCL matrix.

Figure 2c compares the water contact angle of the PCL/HA scaffolds containing different content of HA. The water angle was measured using an automatic contact angle meter (SL200A/B/D Series, Solon Tech. Inc. Ltd., Shanghai, China). As it is seen, the water contact angle decreases from 91.6° for pure PCL to 80.70° for PCL with 15wt% HA, and then increases gradually to 81.4° when the HA content increases further to 25wt%. In all examined samples, the water contact angle on the PCL/HA scaffolds is much smaller than that on the pure PCL. Such result demonstrates that presence of the nano-HA enhances the surface hydrophilicity of the PCL scaffolds [21, 22].

The compressive modulus of PCL/HA scaffolds are measured and shown in Fig. 2d. Here, the scaffolds are fabricated in the form of cylinders (with a diameter of 4 mm and a height of 6 mm) and vertically placed between two parallel plates in a universal testing machine (MTS Industrial Systems Co., Ltd, Shenzhen, China,). A compression rate of 1.0 mm min^{-1} was utilized. Each compressive test was repeated five times. As it is seen, the compressive modulus increases from 112 MPa to 330 MPa when the HA content increases from 0 to 25wt%. In literature, the compressive modulus for pure PCL is measured between 85 MPa and 224.9 MPa [23, 24], which agrees with our measurements. The enhancement is expected as originated from the higher intrinsic mechanical properties of HA (an average compressive strength of 174 MPa and a Young's modulus of 6 GPa) [25], and the uniform distribution of

HA in the PCL matrix which show in the Fig. 1 play a very important role in the mechanical improvement of PCL/HA nanocomposite [24, 26].

The glass transition temperature (Tg) of the PCL/HA scaffold was measured by a differential scanning calorimeter (DSC) (NETZSCH DSC 200 F3, Erich NETZSCH GmbH & Co. Holding KG, Gebrüder-Netzsch-Strasse, Selb, Germany). For pure PCL, the glass transition temperature (Tg) is -66.4°C [27]. Figure 3a shows the DSC curves of PCL and PCL/HA composites, from which the Tg varies from – 70^{o}C to -60^{o}C, suggesting a good compatibility between PCL and HA. According to Fig. 3b, the degradation temperature for weight loss at 10% decreases from 389.7^{o}C to 363.3^{o}C when HA content increases from 0% to 25wt%. Similar result is also observed the degradation temperature for weight loss at 50% (from 515.0^{o}C to 414.0^{o}C). In all, the results from thermogravimetric analysis (TGA) analysis indicate that the addition of HA in PCL decreased the thermal stability of scaffolds as the starting decomposition temperature decreases.

Additionally, the in vitro biocompatibility of the PCL/HA scaffolds was carried out in terms of the proliferation of MC3T3-E1 cells. The osteoblast cells MC3T3-E1 were provided by the China Center for Type Culture Collection of Tongji Medical College, Huazhong University of Science and Technology, and raised according to the method described in literature [19]. In general, no significant differences of cell proliferation activity among all scaffolds are observed after 1 day (Fig. 4.). Whereas, evident differences of cell proliferation activity start to appear among all scaffolds after 3 days. Specifically, PCL/25wt% HA content exhibits the similar cell proliferation activity with the control cells. These results signify that PCL/25wt% HA possesses good biocompatibility and can stimulate cell proliferation well. In all, based on above analysis, PCL/25wt% HA shows the best comprehensive performances and thus being selected to assess their biomedical application potentials.

3.2 In vitro degradation property of PCL/HA scaffolds

Ideally, scaffold materials should be biodegradable during the growth of new bone tissue but maintain good mechanical properties before the bone tissue is completely regenerated. Thus, it is important to understand the biodegradable behaviors of the scaffolds during the degradation for bone regeneration. For such purpose, PCL and PCL/HA scaffolds were suspended in 10 mL of PBS in a dialysis bag and then slowly shaken in 90 mL of phosphate buffer saline (PBS) (pH 7.4) at 37°C. At predetermined time intervals, the samples were taken out of the degradation medium, rinsed with distilled water and then dried in vacuo for 48 h.

As illustrated in Fig. 5a, the number of large pores and cracks increases in the PCL/HA scaffolds when the degradation time increases, and the PCL/HA scaffolds gradually lost their regularity and uniformity. The degradation of the sample can be well reflected by the weight loss and molecular weight loss shown in Fig. 5b and 5c. Compared with pure PCL, the weight loss for PCL/25wt% HA sample is a much smaller during degradation. For instance, after 180 days degradation, the weight losses of pure PCL and PCL/25wt% HA scaffolds are about 10% and 1%, respectively. These results indicate that mass loss occurs at a much lower rate for samples with higher HA content. It is probably that the alkalinity of HA

nanoparticles induces neutralize acidic substances during the degradation of PCL, which resulting in the inhibition of self-acceleration of acidolysis and decreasing of hydrolysis of ester bonds.

The Young's modulus of PCL/25wt% HA content after degradation are measured from tensile experiments and summarized in **Table S2** (see **Supporting Information S2**). It is found that Young's modulus decreases gradually when the degradation time increases from 0 to 4 month, which aligns with the weight loss during the degradation process. It is expected that during the first three months, the degradation processes mainly occur at the end and pendant functional groups of the polymeric chain, and thus result in a minor influence on the molecular chain. After 90 days, the degradation is expected to induce remarkable reduction to the molecular weight of the polymeric main chain and thus results in significant reduction in Young's modulus.

DSC curves of pure PCL and PCL/25wt%HA composites after degradation are also measured and shown in **Fig. S3** (see **Supporting Information S3**). Pure PCL and PCL/HA are found to keep the characteristic peaks of glass-transition temperature varying from − 70℃ to -60℃ after degradation in PBS for months. Specifically, Tg of both samples is found to decrease slightly with the increase of degradation time.

3.3 In vitro drug-release property of PCL/HA scaffolds

To probe the drug-release properties of the PCL/HA composites, Doxorubicin (DOX) were chosen as a model drug and mixed in the samples. DOX is a chemotherapy drug that is used to inhibit the growth of tumors cells [26–29]. In this work, 10 mg of DOX is mixed with each 100 mg of the pure PCL or PCL/HA composite sample. After mixture, the samples were evaporation and then shaped in a disc mold (with a diameter of 10 mm and a height of 2 mm) and suspended in 10 mL of phosphate buffer saline (PBS) (pH 7.4) in a dialysis bag with a continuous shaking for 250 h in the dark environment. The DOX loading capacity was determined using UV-Vis spectrophotometer (UV-2800 series, Unico, Shanghai, China) at 483 nm. The changes of the concentrations of DOX were obtained from curves of the absorption versus concentration of DOX in PBS following the basis of Lambert-Beer law [28].

Recent studies show that the release amount of DOX at first 100 h could reach over 80% [29, 30], such high release rate could inhabit the regeneration of new bone tissue in the tissue engineering. Thus, a controllable release rate is a necessity. Figure 6 compares the DOX-release properties of the pure PCL and PCL/HA scaffolds. After ~ 25 hours (or a day), the DOX-incorporated pure PCL and PCL/HA scaffolds display steady drug-release rates (as indicated by the linear profile of the curves in Fig. 6). Compared with the pure PCL scaffolds, PCL/HA scaffolds exhibit faster drug-release rates, which is suspected as resulted from the increased drug diffusion coefficient (due to the presence of HA). Moreover, the PCL/25wt% HA scaffold show higher release rate than that of the counterpart with 10wt% of HA. After 34 days, the cumulative DOX-release percentage is around 22.0% and 37.7% for the samples with 10wt% and 25wt% of HA, respectively, which is much higher than that of the pure PCL scaffolds (about 10.1%). It is expected that the high content of HA decreases the entanglement degree of PCL, which promotes the DOX release from the scaffolds [31]. Above results suggest that the DOX release rate can be effectively controlled by the content of HA in the PCL/HA scaffolds.

3.4 Cell response of BMSCs of PCL/HA scaffolds

To further elucidate the effect of PCL/HA scaffolds on the differentiation of rat bone marrow-derived mesenchymal stem cells (BMSCs), cell proliferation was evaluated using 3-(4, 5-dimethylthiazol-2-yl)-2, 5-diphenyltetrazolium bromide (MTT) assay after culturing for 1 and 2 days, respectively. Cells adhesion was performed with 4, 6-diamidino-2-phenylindole (DAPI, Sigma) and FITC-Phalloidin (Sigma) as previously described [32]. The expression of osteogenic differentiation related genes and proteins in rat BMSCs cell was also evaluated. The mRNA transcript levels of Actin,alkaline phosphatase (ALP), collagen (COL), runt-related transcription factor-2 (RUNX2), and osteocalcin (OCN) mRNA within rat BMSCs (cultured in different supplemented osteogenic-inducing medium) were assessed by real-time polymerase chain reaction (PCR). In both cases, cells were harvested on day 7 and day 14 then lysed in Trizol (Life Technologies, Carlsbad, CA, USA) and mRNA was extracted according to the manufacturer's protocol. Reverse transcription was carried out using the RNeasy Plus Micro Kit (Hilden, Germany)) and the PCR test was performed using S1000™ Thermal Cycler (Bio-rad, Hercules).

As shown in Fig. 7a, the cell proliferation activity on PCL/25wt% HA scaffolds is obviously higher than the PCL/HA/DOX scaffolds at either day 1 or day 2, whereas the gap between them decreases on day 2. Fluorescence images show that the rat BMSC cells display good adhesion on the surface of the PCL/25wt% HA scaffolds (Fig. 7b), which is beneficial for bone tissue regeneration. From Fig. 7c, PCL/25wt% HA scaffolds support the growth of BMSCs cells and evidently promote the expression of Actin, ALP, COL, RUNX2, OCN mRNA and proteins. The expressions of those genes and proteins are much higher at day 14 than that at day 7. These results demonstrate that the PCL/25wt% HA scaffolds possess good biocompatibility and can stimulate cell proliferation well. Compared with the PCL/25wt% HA scaffolds, the expressions of those genes and proteins are much smaller in the PCL/HA/DOX scaffolds, which is expected as resulted from the quickly released DOX.

3.5 In vivo bone regeneration with skull defect

In vivo bone regeneration ability of PCL/HA scaffolds was investigated by measuring new bone formation using the model of rats with calvarial bone defects. Twelve 6-week-old Sprague-Dawley rats were divided into two groups, with 6 rats in each group. A circular skull defect (with a diameter of 10 mm) was created using a trephine bur (3i Implant Innovation, Palm Beach Gardens, FL, USA) on the left parietal bone of each rat. This size of defect was chosen because it is a defect of this size does not heal by itself without intervention [11]. Thereafter, a circular scaffold (with a diameter of 10 mm and a thickness of 2 mm) was sterilized and implanted into the bone defect location for each rat. To assess the new bone formation in the bone defective area after 4 weeks, micro-computed tomography (micro-CT 50, Scanco Medical AG, Bassersdorf, Switzerland) was utilized under the fixed conditions (24 kV, 2 mA, 90 seconds). The muscle tissues around the scaffolds were taken out and embedded in paraffin and sectioned at a thickness of 5 μm for Hematoxylin-eosin (H&E) staining. The H&E staining slides were visualized under an optical microscope.

According to the micro-CT data, there is no observable new bone formed in the control group with pure PCL scaffolds after 4 weeks post-surgery (see Fig. 8a). In comparison, the group with PCL/25wt% HA shows evident formation of new bone at the edge of the bone defect region (after 4 weeks). In the meantime, there is a certain amount of new bone deposition in the central area of the defects. Further histological analysis affirms the new bone formation after 4 weeks in the group with PCL/25wt% HA scaffolds. These observations signify that the PCL/25wt% HA scaffolds promotes the osteogenic activity, which can repair the bone defect. In the histological analysis,no obvious inflammation was observed in the tissue sections in the H&E staining micrographs after 4 weeks post-surgery (Fig. 8b). This observation further suggests that the PCL/25wt% HA scaffolds possess good biocompatibility and can provide a good microenvironment for osteoblast proliferation and differentiation.

3.6 In vivo bone regeneration with thigh-bone defect

The effects of the scaffolds on bone formation *in vivo* are also evaluated in rabbits with a thigh bone defect in their lower limbs. Eighteen 6-week-old New Zealand white rabbits were divided into three groups with 6 in each group, including the control group (with no scaffold), the group with PCL/25wt% HA scaffolds and the group with PCL/HA/DOX scaffolds. A circular thigh-bone defect (with a diameter of 4 mm) was introduced to the thigh bone of each rabbit. The PCL/25wt% HA and PCL/HA/DOX scaffolds (with a diameter of 4 mm and a height of 6 mm) were firstly coated with collagen I (see **Supporting Information S4**), and then sterilized and implanted into the bone defects for each rabbit following the method used in literatures [33–37]. The implanted position was determined by the magnetic resonance imaging using M7 Small animal MRI system (1.0 Tesla, Aspect Imaging Ltd, Israel) (see **Supporting Information S5**). Area of new bone formation and percentage were measured using the Image Processing and Analysis software taking the femoral implant as the reference baseline. The cylindrical area with a diameter of 4.1 mm and a thickness of 6 mm was set as the three-dimensional reconstruction area of interest. The three-dimensional image was reconstructed with N-Recon software and the three-dimensional analysis was performed with CT-AN software.

As shown in Fig. 9, there is a large amount of new bone formed in the rabbits either with PCL/25wt% HA scaffolds or PCL/HA/DOX scaffolds after 8 weeks. Bone tissues are found to gradually penetrate into the scaffold, adhere on the scaffold surface, and then grow to form a network. Along with the repair process, the PCL/HA scaffolds degrade gradually. These results indicate both PCL/25wt% HA and PCL/HA/DOX scaffolds promote the osteogenic activity and can repair the bone defect. To further assess the new formed bone, Fig. 9b compares bone tissue volume/total tissue volume (BV/TV, %), trabecular thickness (Tb.Th, mm), number of trabecula (Tb.N, mm^{-1}), and bone mineral density (BMD, $g.cm^{-3}$) after 8 weeks surgery. Interestingly, more new bone formation is observed from the rabbit with PCL/25wt% HA scaffolds than the counterpart with PCL/HA/DOX scaffolds after 4 weeks. Probably the large amount of DOX released from the PCL/HA/DOX scaffolds inhibit the cell proliferation activity due to its high cell cytotoxicity to the bone cell. The PCL/25wt% HA scaffolds are found to result in higher bone volume fraction, larger trabecular thickness, larger number of trabecula and higher bone density. It is expected

that, the slowly released DOX at the earlier stage of implantation is conducive to cell proliferation and inhibits inflammation.

4. Conclusions

A multifunctional biodegradable PCL/HA composite was prepared by blending PCL with HA and then the 3D printed PCL/HA scaffolds implants were produced by the screw extrusion/melting deposition forming method using PCL/HA composite as a raw material in this work. *In vitro* assessments reveal that the PCL/HA composite possesses good biodegradability and biocompatibility and promotes cell proliferation. With the addition of a chemotherapy drug (DOX), it is found that the PCL/HA scaffolds has a steady drug release performance, and the release rate can be effectively controlled by the content of HA. Subsequently, *in vivo* experiments for the rats with bone defects and rabbits with skull defect reveal that the PCL/HA scaffolds implants allow the penetration of bone cells, which enables the growth of bone cells and bone tissue regeneration. Therefore the results suggest that PCL/HA composite can be an ideal biodegradable scaffolds for bone repairing after bone malignant tumor resection.

Abbreviations

PCL: poly(ε-caprolactone); HA: hydroxyapatite nanoparticles; DOX: Doxorubicin; ALP: alkaline phosphatase; COL: collagen; RUNX2: runt-related transcription factor-2; OCN: Osteocalcin.

Declarations

Supporting Information

The Supporting Information is available free of charge, including: The thermo properties of pure PCL and PCL/HA scaffolds, degradation property of PCL/HA scaffolds in *vitro*, characterization of PCL/HA/DOX scaffolds coated with collagen I, magnetic resonance imaging of the position of implanted PCL/HA scaffolds in the thigh-bone of rabbit *in vivo*.

Authors' contributions

GY and FLI designed the experiments, FL, ZL, and SJ manufactured and characterized the samples. HK and YS carried out the experiments *in vitro*. FL, HZ and YG wrote the paper and conducted the analysis and discussion, all authors discussed the results and commented on the manuscript. HK and FL contributed equally to this work.

Funding

This work was supported by the National Key R&D Program of China (Grant No. 2018YFB1105502, 2016YFB1101302), Innovative Talents Project of Yellow Crane Talents Plan of Wuhan City (Grant [2017] No.1), Frontier Project of Application Foundation of Wuhan Former Funded Science and Technology Program (Grant No. 2020020601012252), Scientific research projects for high level talents in the new

century of Hubei Province (Grant [2017] No.344), Australian Research Council Discovery Project (Grant No. DP180103009), Scientific Research Fund Project of Wuhan Institute of Technology (Grant No. K201861), and South Hubei Talents Project of Innovation and Entrepreneurship (Grant [2019] No.11). The authors also acknowledge the financial support from the China Scholarship Council (CSC, Grant No. 201908420084).

Availability of data and materials

The data that support the findings of this study are available from the corresponding author upon reasonable request.

Declarations

Ethics approval and consent to participate

All animal experiments were performed at Tongji Hospital of Huazhong University of Science and Technology in accordance with protocols approved by the Institutional Animal Care and Use Committee

Consent for publication

Not applicable.

Competing interests

All authors declare that they have no conflict of interest.

References

1. Matai I, Kaur G, Seyedsalehi A, McClinton A, Laurencin CT. Progress in 3D bioprinting technology for tissue/organ regenerative engineering. Biomaterials. 2020;226:119536.
2. Lian H, Zhang L, Meng Z. Biomimetic hydroxyapatite/gelatin composites for bone tissue regeneration: fabrication, characterization, and osteogenic differentiation in vitro. Materials Design. 2018;156:381–8.
3. McKeea C, Chaudhry GR. Advances and challenges in stem cell culture. Colloid Surface B. 2017;159:62–77.
4. Yan Y, Chen H, Zhang H, Guo C, Yang K, Chen K, Cheng R, Qian N, Sandler N, Zhang YS. Vascularized 3D printed scaffolds for promoting bone regeneration. Biomaterials. 2019;190:97–110.
5. Bunpetch V, Zhang X, Li T, Lin J, Maswikiti EP, Wu Y, Cai D, Li J, Zhang S, Wu C. Silicate-based bioceramic scaffolds for dual-lineage regeneration of osteochondral defect. Biomaterials. 2019;192:323–33.
6. Zhuang P, Sun AX, An J, Chua CK. S. Y. Chew, 3D neural tissue models: From spheroids to bioprinting. Biomaterials. 2018;154:113–33.

7. Daly AC, Pitacco P, Nulty J, Cunniffe GM. D. J. Kelly, 3D printed microchannel networks to direct vascularisation during endochondral bone repair Biomaterials 162 (2018) 34–46.
8. Jang J, Park JY, Gao G, Cho DW. Biomaterials-based 3D cell printing for next-generation therapeutics and diagnostics. Biomaterials. 2018;156:88–106.
9. Hu B, Zhai MY, Yan GP, Zhuo RX, Wu Y, Fan CL. Polycarbonate magnetic microspheres containing tumor necrosis factor-α for potential targeted hepatic carcinoma therapeutics. J Drug Deliv Sci Tec. 2014;24(1):57–60.
10. Hu B, Du HJ, Yan GP, Zhuo RX, Wu Y, Fan CL. Magnetic polycarbonate microspheres for tumor-targeted delivery of tumor necrosis factor. Drug Deliv. 2014;21(3):204–12.
11. Liu D, Nie W, Li D, Wang W, Zheng L, Zhang J, Zhang J, Peng C, Mo X, He C. 3D printed PCL/SrHA scaffold for enhanced bone regeneration. Chem Eng J. 2019;362:269–79.
12. Wang Q, Yang X, Wang G, Wan L, Wang S, Niu X, Wu J, Pan J. Osteogenic growth peptide-loaded 3D-printed PCL scaffolds for the promotion of osteogenesis through the ERK pathway. Materials Design. 2020;193:108811.
13. Güney A, Malda J, Dhert WJ, Grijpma DW. Triblock copolymers based on ε-caprolactone and trimethylene carbonate for the 3D printing of tissue engineering scaffolds. Int J Artif Organs. 2017;40(4):176–84.
14. Huang KH, Lin YH, Shie MY, Lin CP. Effects of bone morphogenic protein-2 loaded on the 3D-printed MesoCS scaffolds. J Formosan Med Assoc. 2018;117(10):879–87.
15. Chen L, Deng C, Li J, Yao Q, Chang J, Wang L, Wu C. 3D printing of a lithium-calcium-silicate crystal bioscaffold with dual bioactivities for osteochondral interface reconstruction. Biomaterials. 2019;196:138–50.
16. Ma H, Feng C, Chang J, Wu C. 3D-printed bioceramic scaffolds: from bone tissue engineering to tumor therapy. Acta Biomater. 2018;79:37–59.
17. Sarkar N, Bose S. Liposome-encapsulated curcumin-loaded 3D printed scaffold for bone tissue engineering. ACS Appl Mater Inter. 2019;11(19):17184–92.
18. Chen H, Yan GP, Li L, Ai CW, Yu XH. Synthesis, characterization, and properties of ε-caprolactone and carbonate copolymers. J Appl Polym Sci. 2009;114(5):3087–96.
19. Li D, Zhang K, Shi C, Liu L, Yan G, Liu C, Zhou Y, Hu Y, Sun H, Yang B. Small molecules modified biomimetic gelatin/hydroxyapatite nanofibers constructing an ideal osteogenic microenvironment with significantly enhanced cranial bone formation. Int J Nanomed. 2018;13:7167.
20. Lu K, Yan G, Chen H, Li L, Ai C, Yu X. Microwave-assisted ring-opening copolymerization of □-caprolactone and 2-phenyl-5,5-bis(oxymethyl) trimethylene carbonate. Chin Sci Bull. 2009;54(18):3237–43.
21. Xia Y, Zhou P, Cheng X, Xie Y, Liang C, Li C, Xu S. Selective laser sintering fabrication of nano-hydroxyapatite/poly-ε-caprolactone scaffolds for bone tissue engineering applications. Int J Nanomed. 2013;8:4197.

22. Medeiros GS, Muñoz PA, de Oliveira CF, da Silva LC, Malhotra R, Gonçalves MC, Rosa V, Fechine GJ. Polymer nanocomposites based on poly (ε-caprolactone), hydroxyapatite and graphene oxide. J Polym Environ. 2020;28(1):331–42.
23. Li Y, Han C, Yu Y, Xiao L. Effect of loadings of nanocellulose on the significantly improved crystallization and mechanical properties of biodegradable poly(ε-caprolactone). Int J Biol Macromol. 2020;147:34–45.
24. Choi WY, Kim HE, Oh SY, Koh YH. Synthesis of poly (ε-caprolactone)/hydroxyapatite nanocomposites using in-situ co-precipitation. Mat Sci Eng C Mater. 2010;30(5):777–80.
25. Martin R, Brown P. Mechanical properties of hydroxyapatite formed at physiological temperature. J Mater Sci Mater Med. 1995;6(3):138–43.
26. Corcione CE, Gervaso F, Scalera F, Padmanabhan SK, Madaghiele M, Montagna F, Sannino A, Licciulli A, Maffezzoli A. Highly loaded hydroxyapatite microsphere/PLA porous scaffolds obtained by fused deposition modelling. Ceram Int. 2019;45(2):2803–10.
27. Ramírez Agudelo R, Scheuermann K, Gala García A, Monteiro APF, Pinzón García AD, Cortés ME, Sinisterra RD. Hybrid nanofibers based on poly-caprolactone/gelatin/hydroxyapatite nanoparticles-loaded doxycycline: effective anti-tumoral and antibacterial activity. Mat Sci Eng C Mater. 2018;83:25–34.
28. Javanbakht S, Namazi H. Doxorubicin loaded carboxymethyl cellulose/graphene quantum dot nanocomposite hydrogel films as a potential anticancer drug delivery system. Mat Sci Eng C Mater. 2018;87:50–9.
29. Kozlu S, Sahin A, Ultav G, Yerlikaya F, Calis S, Capan Y. Development and in vitro evaluation of doxorubicin and celecoxib co-loaded bone targeted nanoparticles. J Drug Deliv Sci Tec. 2018;45:213–9.
30. Lai YL, Cheng YM, Yen SK. Doxorubicin-chitosan-hydroxyapatite composite coatings on titanium alloy for localized cancer therapy. Mat Sci Eng C Mater. 2019;104:109953.
31. Ouyang L, Sun Z, Wang D, Qiao Y, Zhu H, Ma X, Liu X. Smart release of doxorubicin loaded on polyetheretherketone (PEEK) surface with 3D porous structure. Colloid Surface B. 2018;163:175–83.
32. Sun Y, Kang H, Lin K, Guan H, Liu J, Li F. Evaluation of mechanical properties and osteogenesis ability of porous titanium alloy scaffolds manufactured by selective laser melting technique. Orthop Biomech Mater Clin Study. 2019;016(002):1–5.
33. Du YW, Zhang LN, Hou ZT, Ye X, Gu HS, Yan GP, Shang P. Physical modification of polyetheretherketone for orthopedic implants. Front Mater Sci. 2014;8(4):313–24.
34. Du YW, Zhang LN, Ye X, Nie HM, Hou ZT, Zeng TH, Yan GP, Shang P. In vitro and in vivo evaluation of bone morphogenetic protein-2 (BMP-2) immobilized collagen-coated polyetheretherketone (PEEK). Front Mater Sci. 2015;9(1):38–50.
35. Feng P, Wu P, Gao C, Yang Y, Guo W, Yang W, Shuai C. A multimaterial scaffold with tunable properties: toward bone tissue repair. Adv Sci. 2018;5(6):1700817.

36. Liu Y, Li T, Ma H, Zhai D, Deng C, Wang J, Zhuo S, Chang J, Wu C. 3D-printed scaffolds with bioactive elements-induced photothermal effect for bone tumor therapy. Acta Biomater. 2018;73:531–46.
37. Shi F. Medical animal experiment method, China. Beijing: People's Medical Publishing House; 1990.

Figures

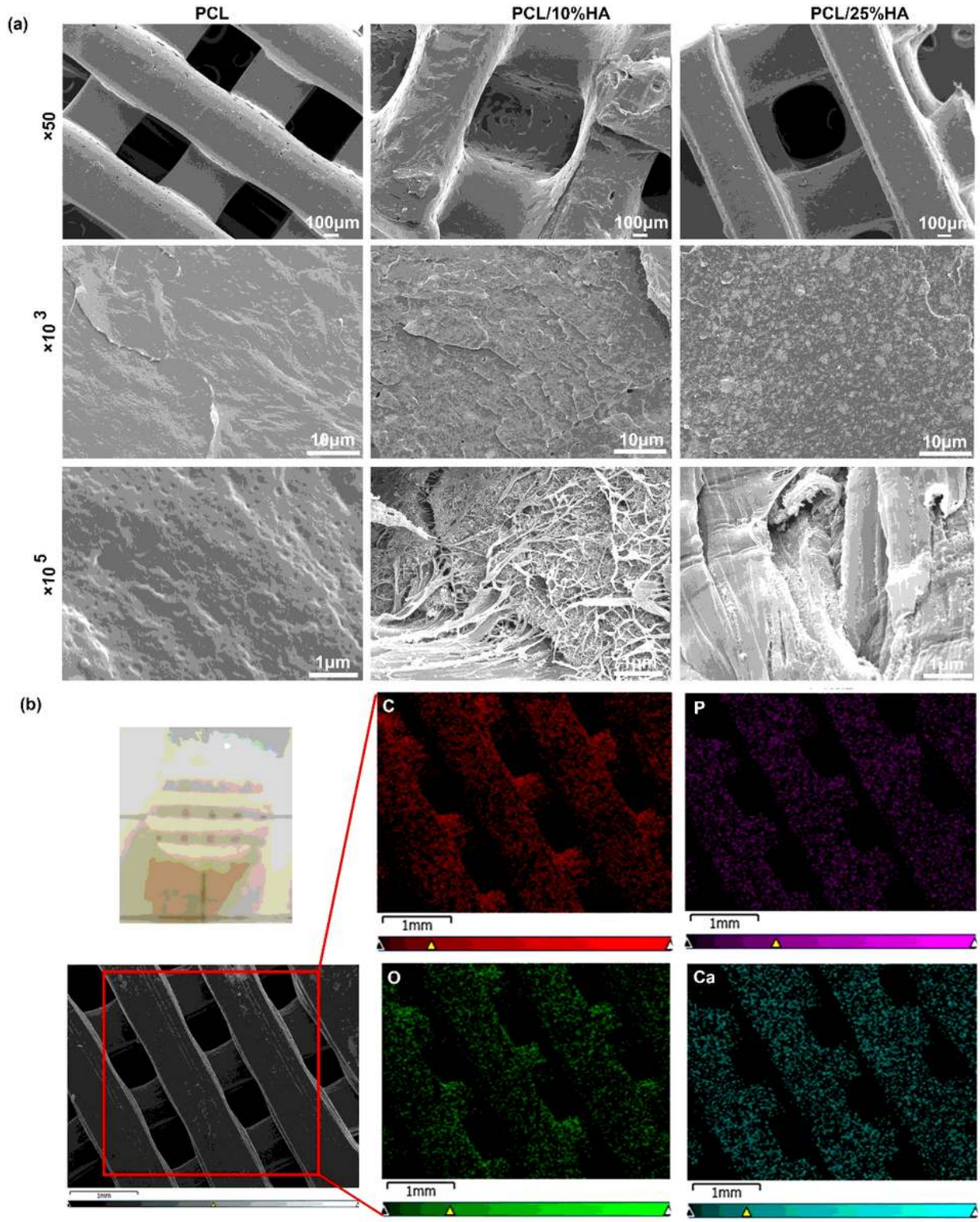

Figure 1

The characteristics of scaffolds. (a) Micromorphology of PCL/HA scaffolds in different content (0%, 10wt%, 25wt%) (upper panel: ×50, middle panel: ×103, lower panel: ×105); (b) The optical graphs and EDS mapping distribution of C, O, Ca, and P elements in the surface of PCL/25wt% HA scaffolds.

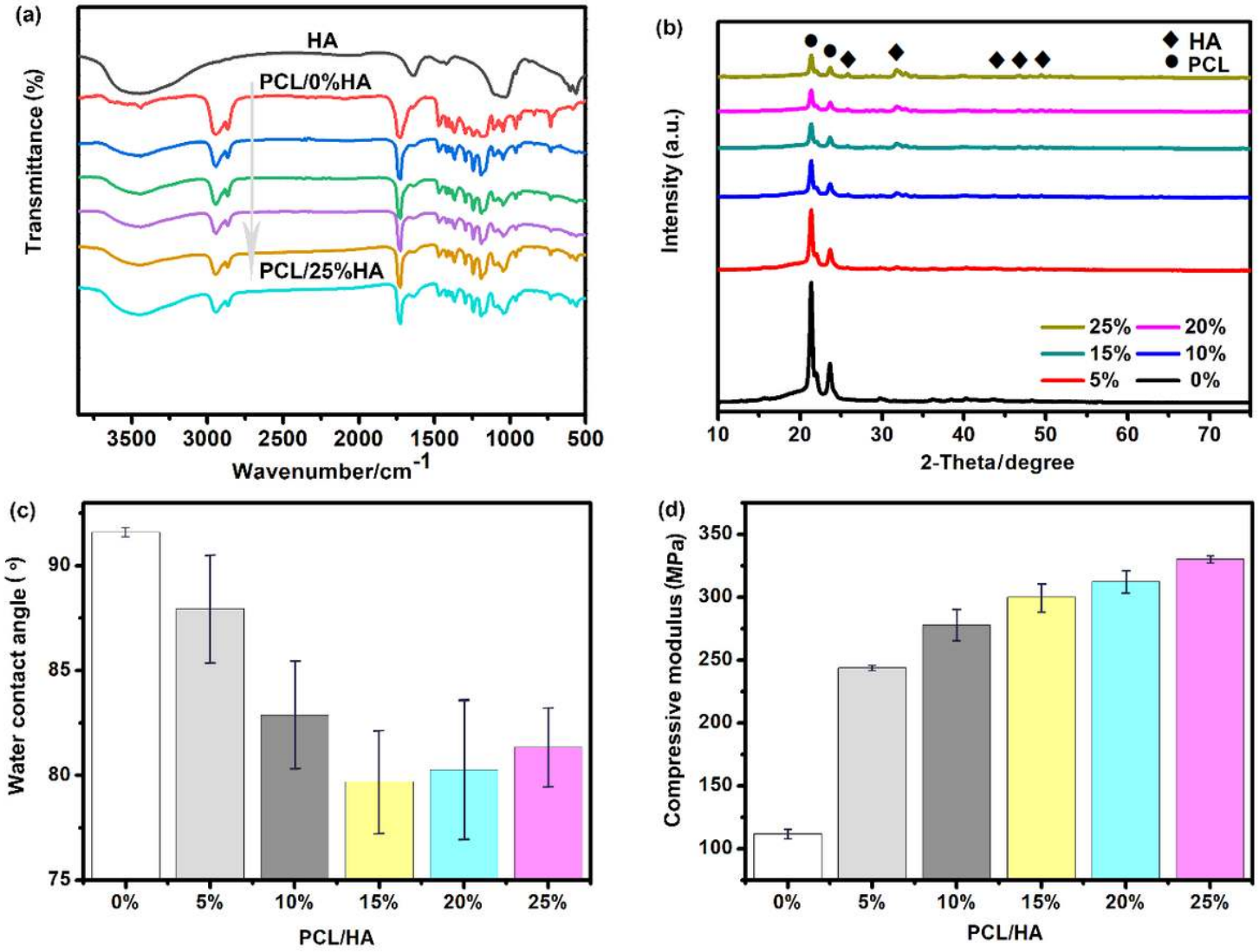

Figure 2

Characterization of different PCL scaffolds with different content of HA ranging from 0% to 25wt%. (a) FT-IR result; (b) XRD spectra; (c) Water contact angle as a function of the HA content; and (d) Compressive modulus as a function of the HA content.

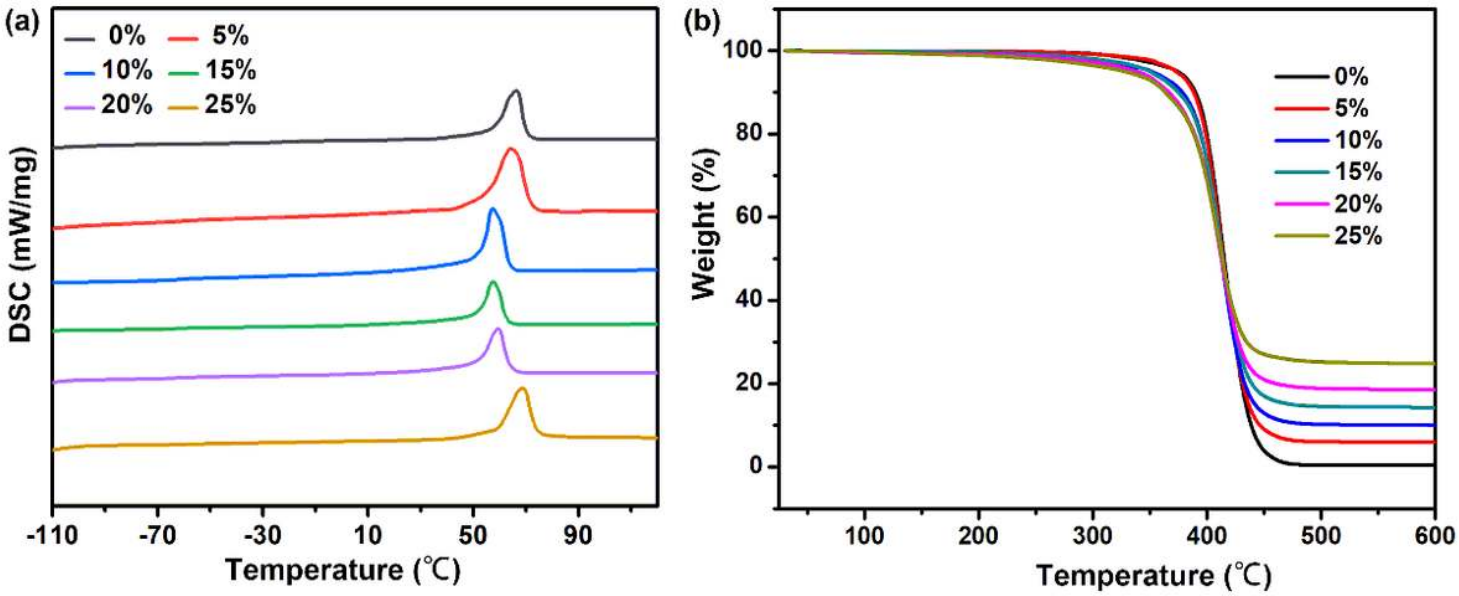

Figure 3

The thermal properties of the PCL scaffolds with different HA contents. (a) DSC profiles for the PCL/HA composite with different content of HA; (b) Thermogravimetric-differential thermal analysis curves of PCL/HA scaffolds.

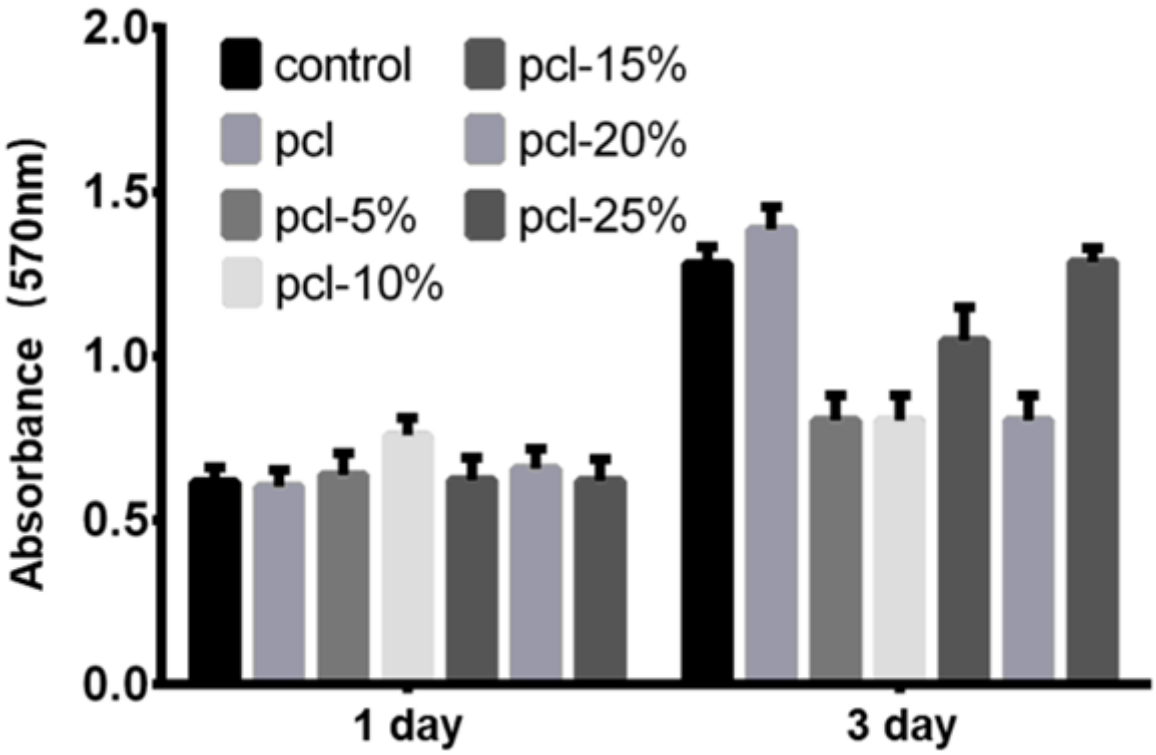

Figure 4

Cell proliferation results of MC3T3-E1 cells after culturing for 1 and 3 days on the PCL/HA scaffolds with 0%-25wt% content of HA

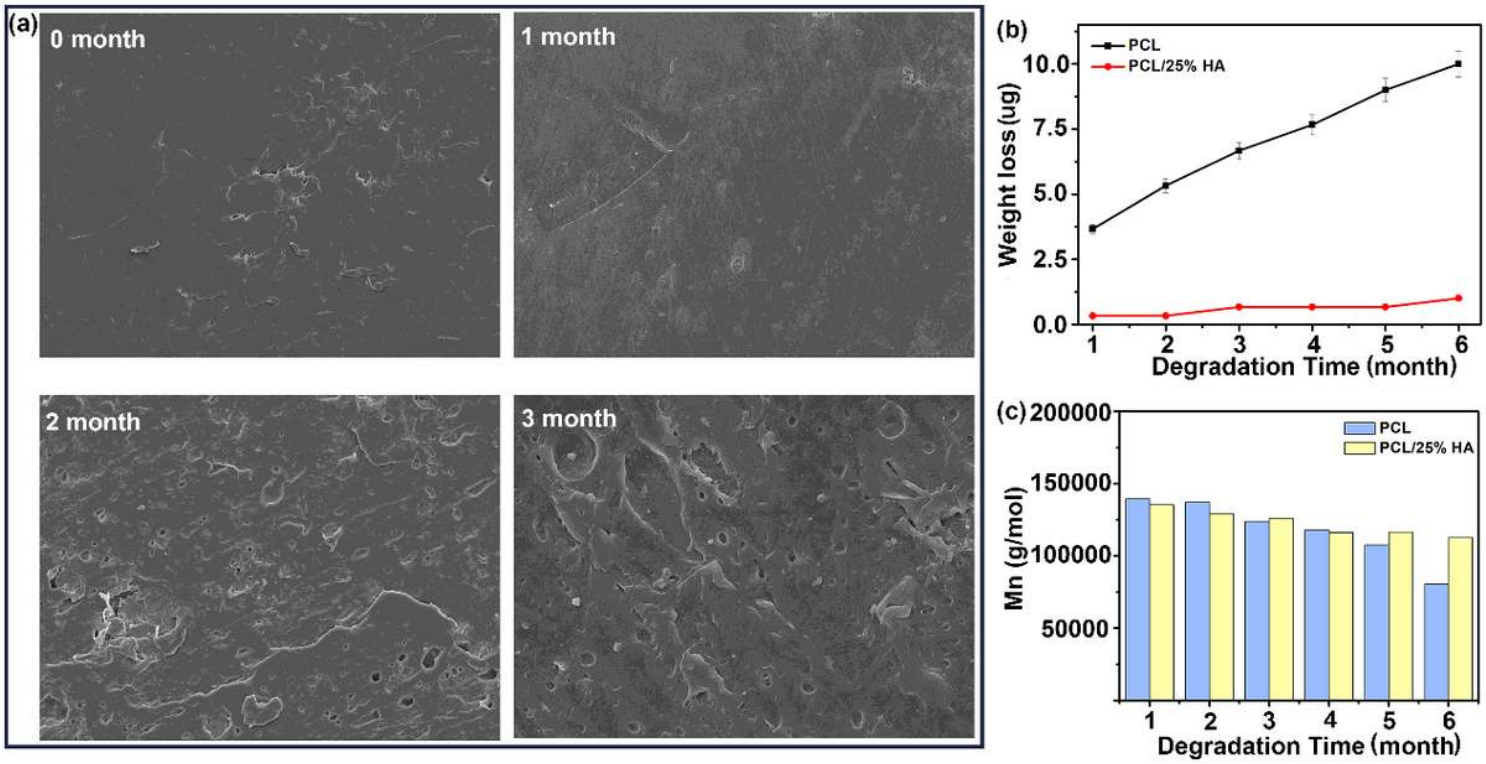

Figure 5

The degradation behaviors of the PCL/25wt% HA scaffolds after PBS immersion. (a) SEM micrographs of the scaffolds with PCL/25wt% HA scaffolds after PBS immersion for 3 months; (b) Weight loss and weight-average molecular weight (Mn) of the PCL scaffold with 0%, 25wt% of HA content for six months.

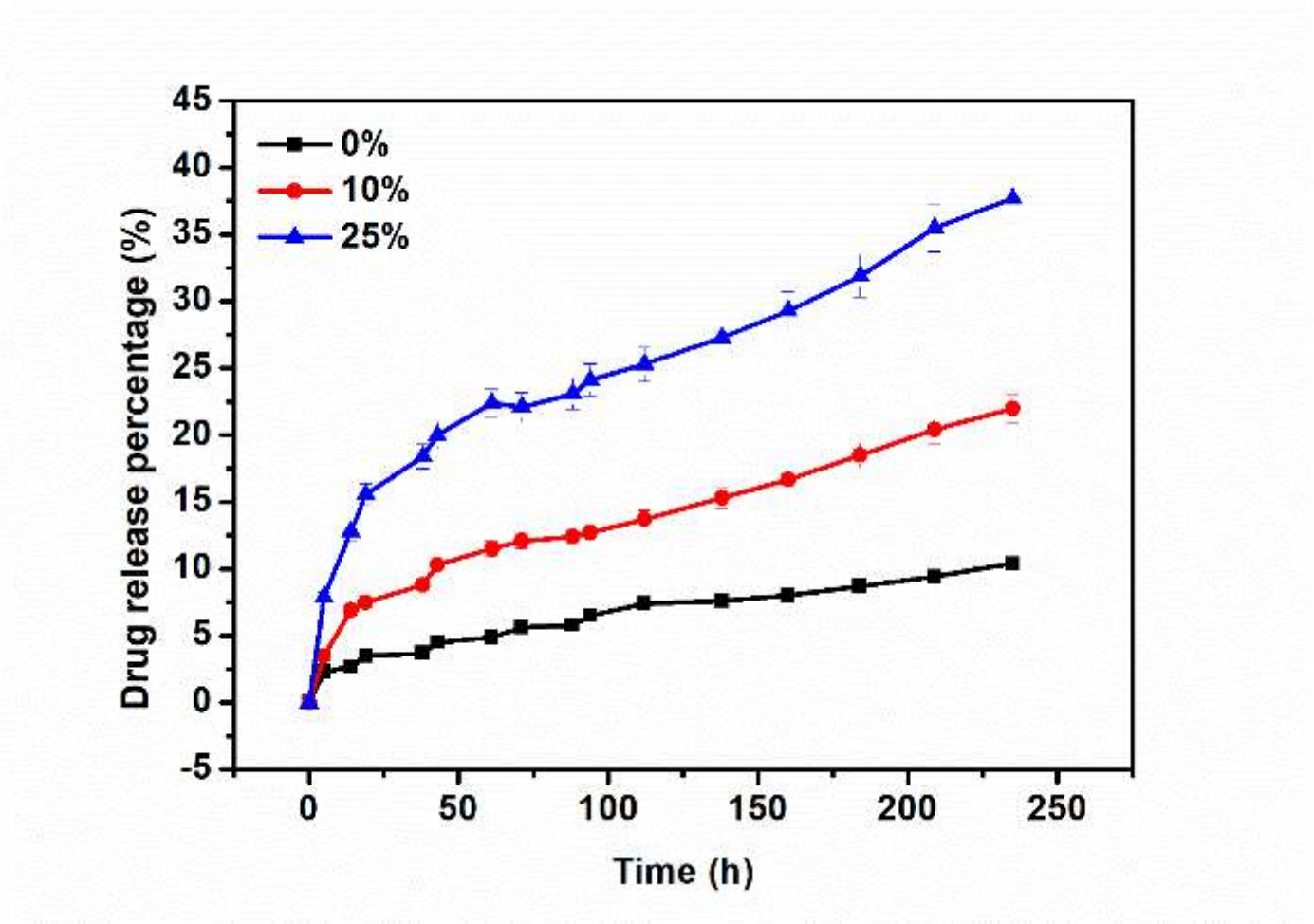

Figure 6

Release profiles of DOX-incorporated PCL scaffold with 0%, 10%, 25wt% of HA content for 250 h.

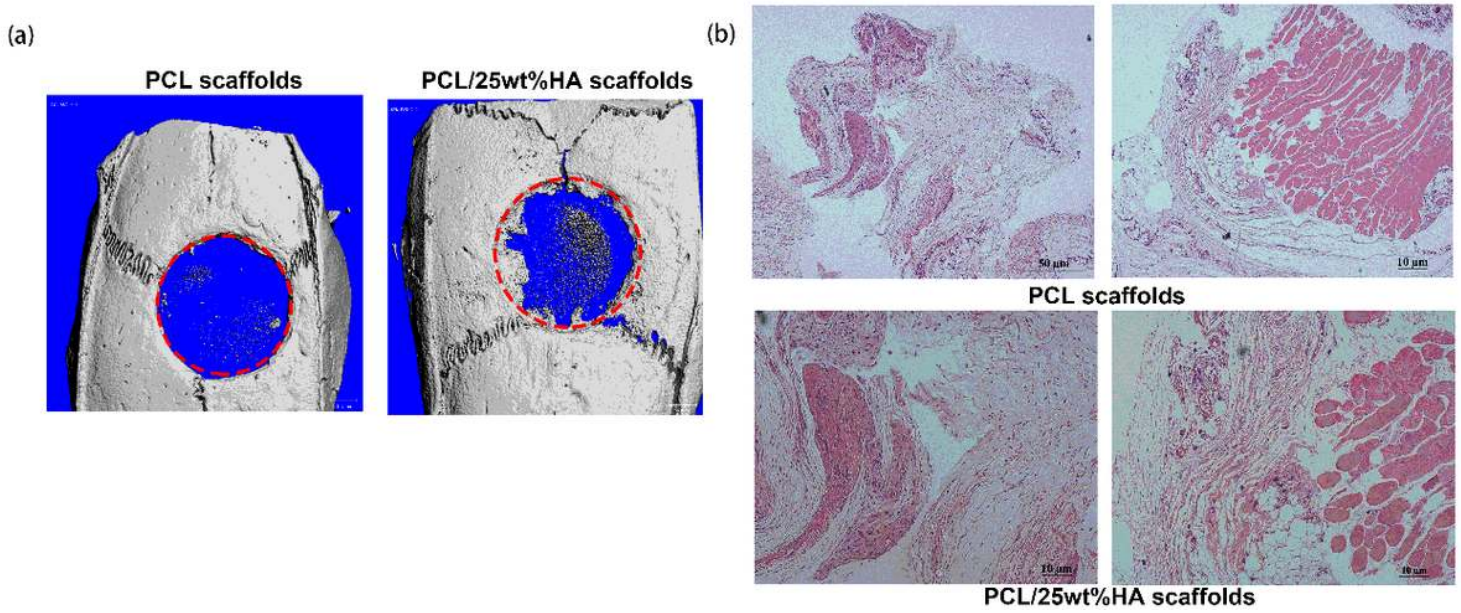

Figure 8

In vivo micro-CT images and histological analysis in skull defect. (a) Micro-CT of the skull defect repair in rats with pure PCL and PCL/25wt% HA scaffolds at 4 weeks; (b) H&E staining of the muscle on the back of the rats at 4 weeks post-surgery (HE ×300).

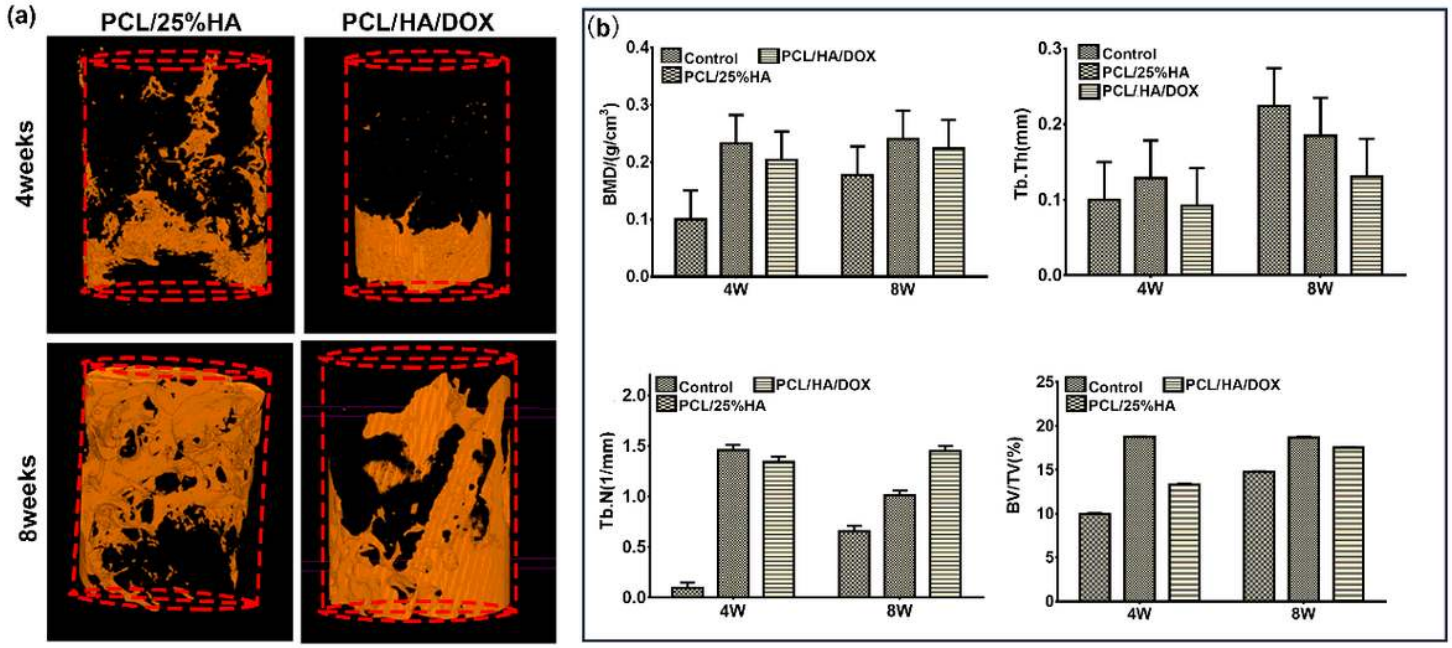

Figure 9

Micro-CT analysis of the effect of scaffolds on thigh-bone defect in vivo. (a) Representative three-dimensional reconstructed micro-CT images showing the effect of PCL/HA scaffolds on the new bone tissue formation inside the defect site (red dashed line). (left: PCL/25wt% HA scaffolds for 4 weeks and 8 weeks, right: PCL/HA/DOX scaffolds for 4 weeks and 8 weeks); (b) Summarized data showing the micro-architectural parameters of the new formed bone tissue at 4 and 8 weeks by analyzing the three-dimensional reconstructed micro-CT images using image analysis software. BMD, BV/TV, Tb.Th and Tb.N were shown in the panel.

Supplementary Files

This is a list of supplementary files associated with this preprint. Click to download.

- supplementaryinformation20210507.docx